

# Tubular Crystals of Acetylcholine Receptor

A. BRISSON and P. N. T. UNWIN

Laboratoire de Biologie Moléculaire et Cellulaire, Centre National de la Recherche Scientifique E. R. 199, Département de Recherche Fondamentale, Centre d'Etudes Nucleaires, Grenoble 38041 France; and Department of Structural Biology, Stanford University School of Medicine, Stanford, California 94305

**ABSTRACT** Well-ordered tubular crystals of acetylcholine receptor were obtained from suspensions of *Torpedo marmorata* receptor-rich vesicles. They are composed of pairs of oppositely oriented molecules arranged on the surface lattice with the symmetry of the plane group p2 (average unit cell dimensions:  $a = 90 \text{ \AA}$ ,  $b = 162 \text{ \AA}$ ,  $\gamma = 117^\circ$ ). The receptor in this lattice has an asymmetric distribution of mass around its perimeter, yet a regular pentagonal shape; thus its five transmembrane subunits appear to have different lengths, but approximately equal cross sections. The tubes grow by lateral aggregation on the vesicle surface of ribbons of the paired molecules. Both ribbons and tubes were sensitive to dispersal by the disulphide reductant, dithiothreitol. This observation and other evidence suggest that the basic pairing interaction in the tubes may be that of the physiological dimer, involving contact between  $\delta$ -subunits.

Nerve cells transfer signals at chemical synapses by releasing neurotransmitters from their terminal regions and inducing a change in the permeability to ions of specific receptors in the postsynaptic membranes of communicating cells. The nicotinic acetylcholine receptor is an example of such a receptor. It is a pentameric membrane protein composed of four polypeptide chains, assembled with the stoichiometry  $\alpha_2\beta\gamma\delta$  (reviewed in references 6, 8, 16, 22). The amino acid sequences deduced from recent cDNA sequences (7, 10, 19, 20) indicate molecular weights of 50,000 ( $\alpha$ ), 54,000 ( $\beta$ ), 56,000 ( $\gamma$ ), and 58,000 ( $\delta$ ), and show considerable homology between the chains (21, 23). The assembly in the bilayer forms a ring, the central axis of which is thought to delineate the ion-selective channel (4, 18). In the native membranes of *Torpedo* electroplaques, these molecules normally exist as dimers, paired through disulphide bonds between the  $\delta$ -subunits (5, 14). Dimers of receptors, often grouped in double rows, can be seen in quick-frozen deep-etched postsynaptic membranes of the electroplaque (15).

The acetylcholine receptor is unique among all receptors in the extent to which its biochemical and pharmacological properties have been characterized, yet little direct information is available concerning its three-dimensional structure. Crystallographic analysis has been carried out of membrane-bound receptors ordered in planar sheets (24) and in tubes (3, 17); also, images of individual receptors have been enhanced by correlation averaging (27, 28). However, the resolution and accuracy of the molecular details so far obtained have been limited by the quality of such preparations.

We report here on the properties of tubular crystals grown in suspensions of receptor-rich vesicles, which were prepared from the electric organ of *Torpedo marmorata*. Tubes apparently form by lateral aggregation on the vesicle surface of ribbons of paired receptor molecules, morphologically similar to those found on quick-frozen postsynaptic membranes. Image analysis of selected tubes enabled us to derive a map of the structure of the receptor in projection.

## MATERIALS AND METHODS

**Isolation of Acetylcholine Receptor-rich Vesicles:** Membranes enriched in receptors were prepared from freshly killed and dissected *Torpedo marmorata* (Marine Station, Arcachon, France). Typically, 80 g of electric organ was cut into small pieces, washed, and then homogenized (Sorvall omni-mixer [E. I. Dupont de Nemours & Co., Inc., Newton, CT]; 2 min at maximum speed) using 135 ml of isolation buffer (400 mM NaCl, 50  $\mu$ M phenylmethylsulphonyl fluoride, 20 mM phosphate buffer, pH 7.4). After centrifugation (6,000 rpm for 10 min in a Sorvall JA-14 rotor), the supernatant was passed through two layers of cheesecloth. The filtrate was centrifuged (20,000 rpm for 30 min in a Beckman Ti45 rotor [Beckman Instruments, Inc., Palo Alto, CA]) which produced a pellet consisting of a loose white layer overlying a small, yellowish compacted base. The upper layer was resuspended in 40 ml of isolation buffer, using a Potter homogenizer (Arthur H. Thomas Co., Philadelphia, PA) with a tightly fitting teflon pestle, and centrifuged again (30,000 rpm for 40 min in a Beckman Ti45 rotor). The second high-speed pellet was resuspended as before in 20 ml of crystallization buffer (100 mM Tris-HCl, pH 6.8) and then diluted further to  $\sim 1 \text{ mg/ml}$  (total protein) to yield the final vesicle-containing suspension. This suspension contained a significant proportion of nonreceptor material. However, additional purification by, for example, sucrose gradient centrifugation, did not lead to enhancement of tube formation and therefore was not routinely carried out. All steps of the isolation

procedure were carried out at 4°C, using reagent grade chemicals and double distilled water.

**Crystallization:** 2-ml aliquots of the final vesicle-containing suspension were diluted in crystallization buffer over a  $\times 10$  range and incubated in sealed glass bottles at temperatures of 4–17°C. Solutions were monitored by withdrawing  $\sim 20\text{-}\mu\text{l}$  samples every 2 or 3 d and examining the contents by electron microscopy using negative stain. Tubes appeared reproducibly within these temperature/dilution ranges after a period of 3–4 wk.

**Electron Microscopy and Image Processing:** Specimens were applied to freshly glow-discharged carbon support grids and negatively stained with 2% sodium phosphotungstate (pH 7.2). They were examined at 100 kV with a Philips EM400 electron microscope equipped with a low-dose kit. Electron micrographs were recorded on Kodak S0163 film at a magnification of 28,500 and with a total electron dose of less than five per square angstrom. The magnification was calibrated using negatively stained catalase crystals as a standard (26). Films were developed in full strength Kodak D19 developer for 8 min.

Preliminary assessment of the tube images was by optical diffraction. We saw two kinds of diffraction maxima: a set of strong peaks arranged on a near-to-hexagonal lattice and a set of weak "superlattice" peaks at points midway between the strong ones. Several of the "superlattice" peaks became more prominent relative to the others when the tubes were tilted (Fig. 1); however, they were still visible without any tilting—the view we consider in this paper. The presence of the "superlattice" peaks, and a high degree of mirror symmetry about a vertical axis (see Fig. 7), were taken to indicate good preservation of the untilted tubes. Uniform staining and low electron doses were needed to reveal and retain these features.

Further analysis of the best-preserved tubes was by computer. Selected areas were converted into two-dimensional arrays of optical densities by using an automatic microdensitometer (Perkin-Elmer Corp., Eden Prairie, MN) with step and spot sizes of  $25\ \mu\text{m}$  (equivalent to  $8.77\ \text{\AA}$  at the specimen). These arrays were made up to a standard size of  $512 \times 256$ . Fourier transformation and synthesis calculations were then carried out as described (9, 25) to provide single-side filtered images and projection maps.

In deriving filtered images we made the mask size in the computed transform sufficiently large to include all the intensity associated with each peak. This enabled us to examine closely the structural variation across the width of a tube, due, for example, to non-uniform or incomplete flattening. Based on the lateral variation of the stain and the projected center-to-center separation of individual molecules, the flattening appeared to be asymmetric, as found with large spherical viruses observed in similar conditions (11). Most frequently the cross section appeared to be of the form shown in Fig. 2, although an exact

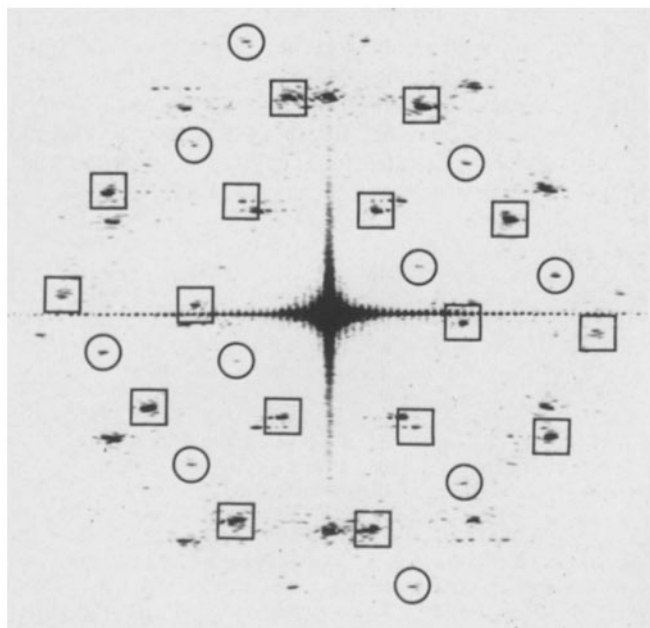


FIGURE 1 Optical transform from a tube tilted by  $23^\circ$  to the incident electron beam. Peaks from just one side have been outlined to show "superlattice" peaks (circles) which lie at positions midway between the major peaks (squares). Several of the "superlattice" peaks become slightly stronger upon tilting, which makes them more visible than they are in the transforms from untilted tubes (Fig. 7). Scale:  $1\ \text{cm} = 0.0076\ \text{\AA}^{-1}$ .

profile can only be guessed at. Supporting this deduction, stain accumulation was usually greatest near the edge of a tube, rather than near the middle (as it would be if the cross section were an ellipse), the separation and stained appearance of molecules was more variable on one side of a tube than the other, and the separation of molecules on the variable side was greatest in a zone near the edge. By comparing filtered images of the same tubes tilted in a particular sense by two different angles, we determined which side was uppermost (i.e., nearest the electron source) and hence the absolute hand of the surface lattice (see Fig. 8B). This experiment confirmed that the side facing the carbon support was generally the most uniform one; it was also the least sensitive to radiation damage (results not shown). For subsequent analysis we selected only the uniformly flattened sides of tubes.

Fourier transforms were computed from the central ( $\sim 2,500 \times 800\ \text{\AA}^2$ ) regions (see Fig. 2), giving single sharp peaks which we fitted by a least squares procedure to a regular two-dimensional net. Examples of single-side transforms were thus obtained in which no peaks deviated from the net points by more than  $\sim 3\%$  of the unit cell dimensions of the net (Table I). The accuracy of this fit is comparable to that of extensive crystalline sheets (see reference 1). Projection maps were derived from such examples, using the amplitude and phase values collected at the net points (25). Peaks were well sampled because the transform dimensions were typically about four times that of the image density array. Those peaks with amplitudes less than 1.5 times the mean background level were excluded from the synthesis, and transforms were not used if net points corresponding to the two sides of a tube overlapped.

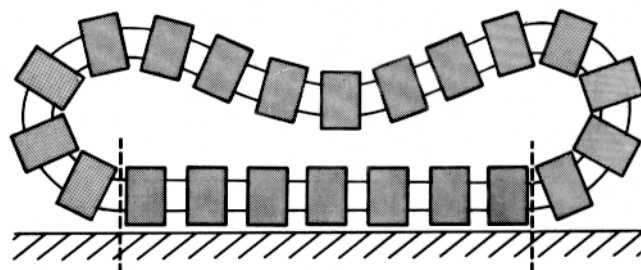


FIGURE 2 Schematic diagram of the likely cross section of many of the tubes, as suggested by the stain distribution and projected center-to-center separation of individual molecules seen in filtered images. Examples were found in which the side facing the carbon support film (bottom) appeared uniformly flat and evenly stained over the entire region within the vertical broken lines; structure factors (Table I) and projection maps (Fig. 9) were derived from such regions.

## RESULTS

### Formation of Tubes

Vesicles initially were  $0.5\text{--}1.5\ \mu\text{m}$  diam with receptors densely packed but apparently organized randomly over their surfaces. The first clearly identifiable aggregates were observed only after periods of incubation (see Materials and Methods) of 3–4 wk. These consisted of paired molecules aligning linearly and forming double rows or ribbons over the vesicle surface (Fig. 3). Short, poorly ordered tubes were also produced at this stage (Fig. 4a). After a further 1–2 wk the tubes became better ordered and longer (up to  $3\ \mu\text{m}$ ; Fig. 5), and their width remained fairly constant ( $800\text{--}1,200\ \text{\AA}$ ). Accompanying elongation, the size of the nontubular regions tended to become smaller, as if receptors in the crystalline lattice were being recruited from those already present in the same vesicle.

A characteristic feature of the tubes is the extensive striated zone that appears at their edges (Figs. 4b, 5, and 6) (3, 17). This corresponds to protein protruding from the membrane and indicates that the receptor is oriented on the tube surface with its synaptic (i.e., extracellular) side pointing outwards (17, 18).

Both ribbons and tubes dispersed completely after incubation (8 h at 4°C) with small amounts (1 mM) of dithiothreitol,

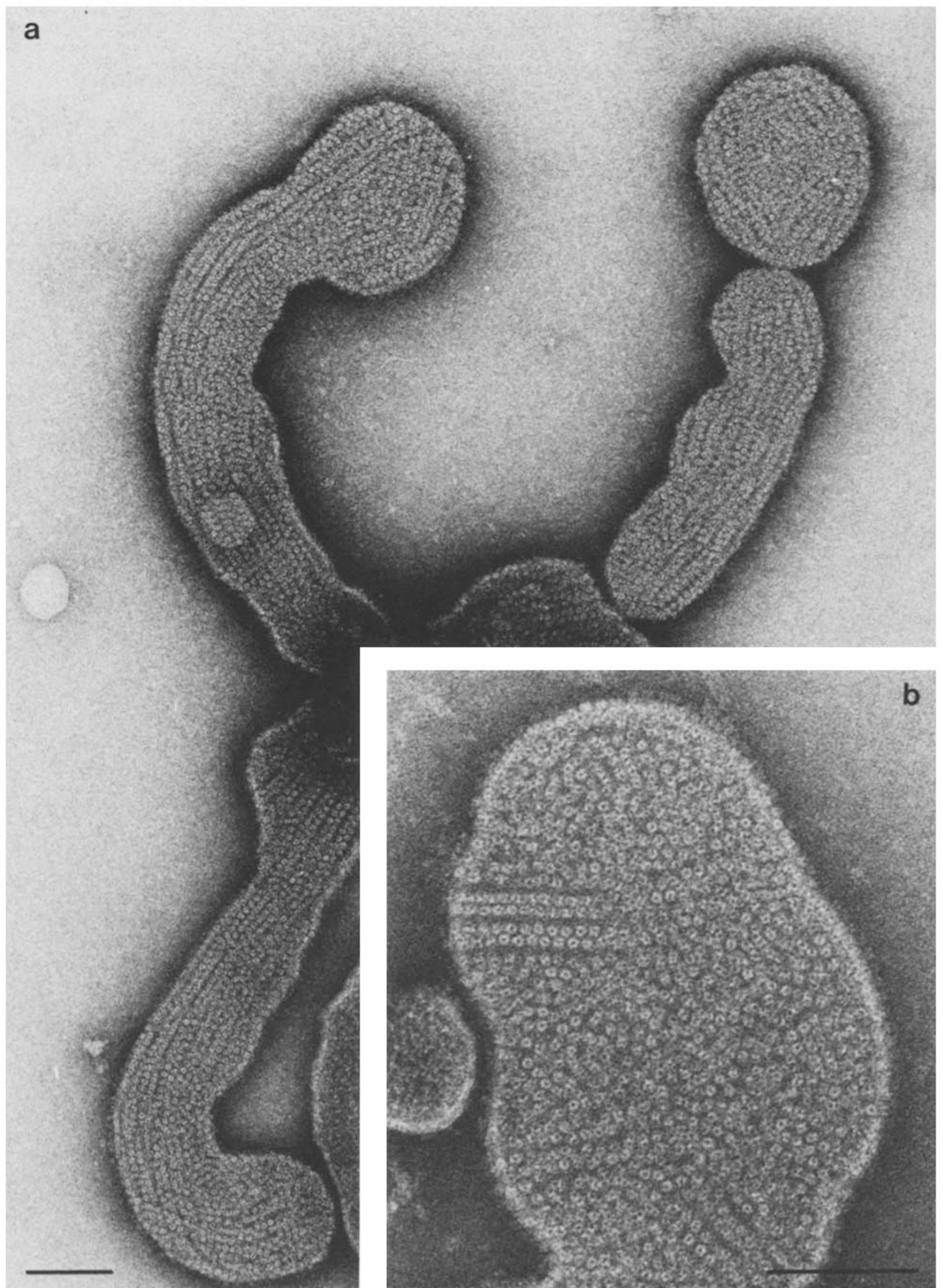


FIGURE 3 . Vesicles with ribbons of paired receptors extending across their surfaces. The incubation conditions were 3 wk at 17°C. Bar, 0.1  $\mu\text{m}$ .  $\times$  150,000. (inset) Bar, 0.1  $\mu\text{m}$ .  $\times$  270,000.

TABLE I  
Structure Factors and Location Errors of Transform Peaks from Flattened Tubes

h	k	Tube A				Tube B			
		Amplitude	Phase*	$\delta Y^\dagger$	$\delta X$	Amplitude	Phase	$\delta Y$	$\delta X$
-1	4	12.1	4	-0.00002	0.00006	13.3	0	0.00001	0.00013
0	2	9.5	185	0.00002	0.00006	8.2	185	0.00005	-0.00010
0	3	1.3	143	0.00006	-0.00023	2.4	182	-0.00007	0.00028
0	4	8.7	186	-0.00001	0.00003	10.3	181	0.00004	-0.00005
1	-2	9.1	356	0.00004	0.00019	6.0	7	0.00001	0.00023
1	-1	4.2	353	-0.00001	-0.00013	3.0	4	-0.00003	0.00025
1	0	13.0	187	0.00002	0.00011	11.6	184	-0.00000	-0.00002
1	2	8.8	179	0.00001	-0.00031	10.9	179	0.00000	0.00003
1	3	3.2	178	-0.00001	0.00002	3.0	170	0.00001	0.00015
2	-4	6.3	181	0.00002	0.00014	7.2	185	-0.00002	0.00000
2	-3	5.4	182	0.00000	-0.00015	4.6	182	0.00004	-0.00013
2	-2	9.0	1	-0.00002	-0.00001	8.5	358	0.00000	-0.00005
2	0	8.0	184	0.00000	0.00011	9.0	181	0.00001	0.00010
3	-2	1.4	171	-0.00001	0.00003	2.0	162	0.00001	0.00012

\* Refined to nearest real values, 0° and 180°; average deviations from these values are 6.5° and 4.9° for tubes A and B, respectively.  
 $\dagger$  Deviations of peaks from points on two-dimensional net in directions parallel ( $\delta Y$ ) and perpendicular ( $\delta X$ ) to the tube axis; in  $\text{\AA}^{-1}$ .

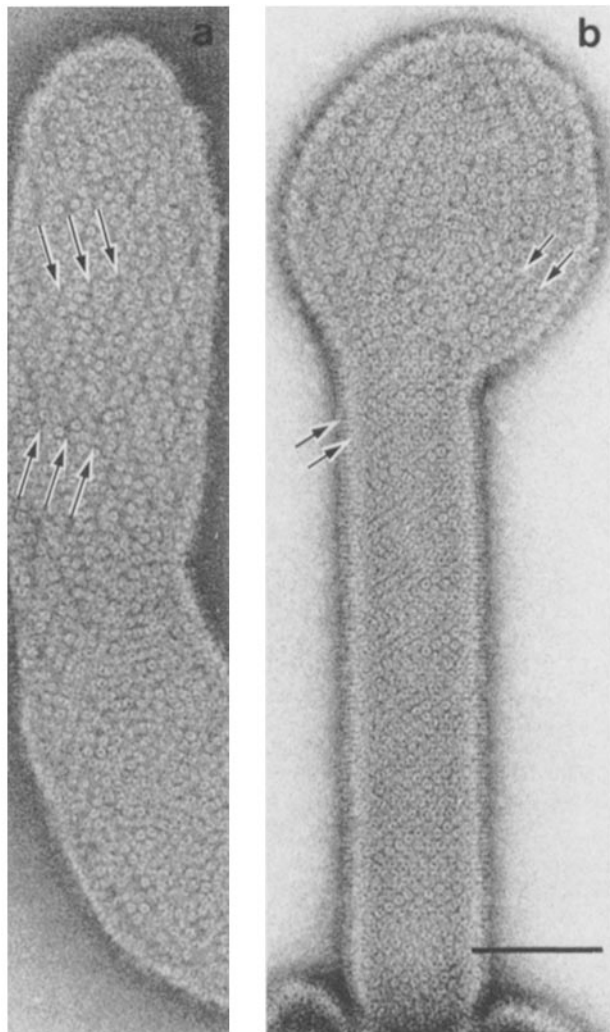


FIGURE 4 Details on vesicle surfaces apparently relating ribbons of paired receptors to packing in tubes. (a) Ribbons are aligned obliquely (arrows) to the axis of an elongated vesicle, creating a loosely packed tubular surface lattice. (b) Rows of receptors in the terminal part of a tube are aligned with ribbons present in the rounded end region. This can be seen most clearly by viewing at glancing angle along the direction of the arrows. Bar, 0.1  $\mu\text{m}$ .  $\times 177,000$ .

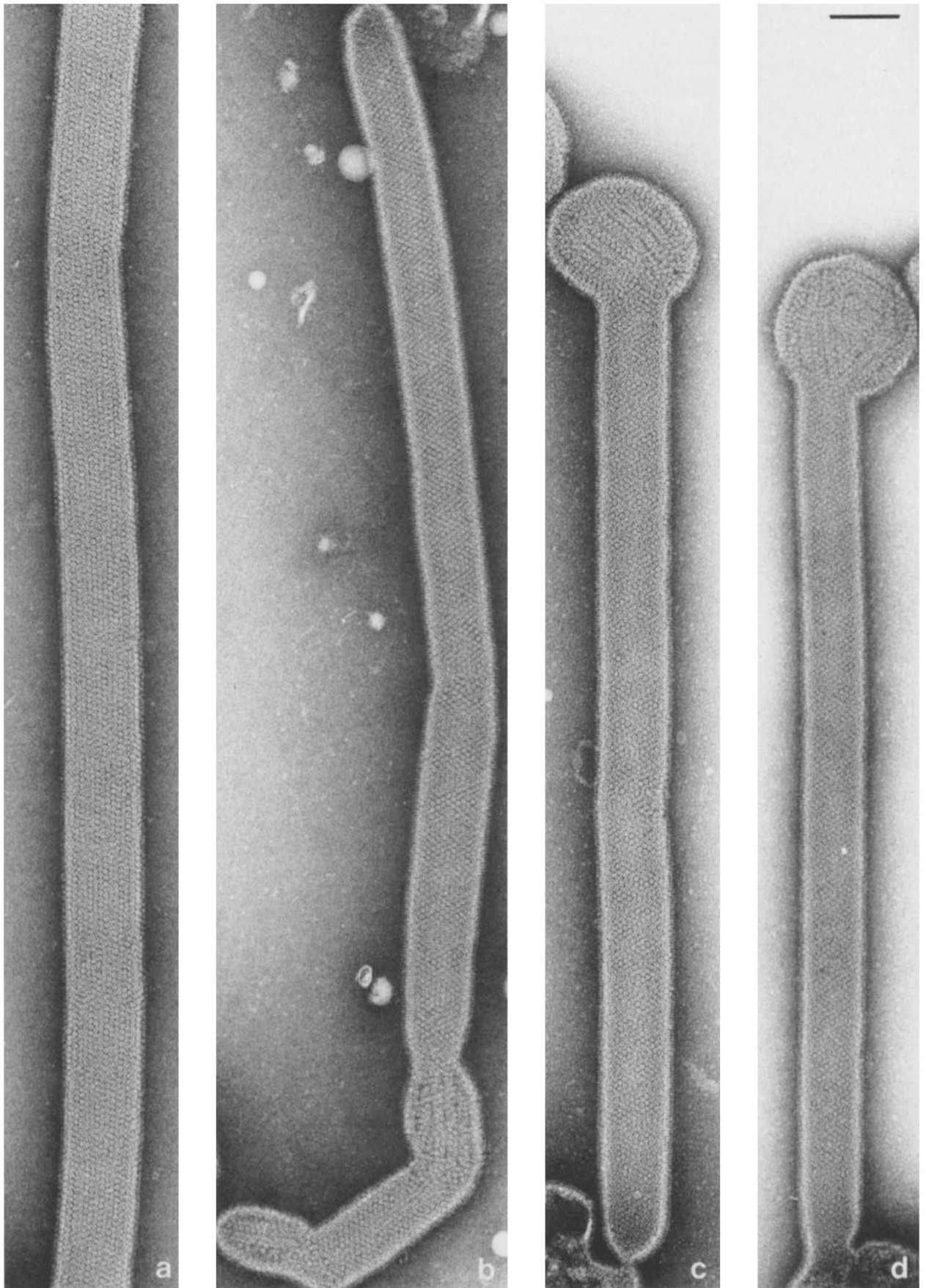


FIGURE 5 Mature tubes obtained after incubation for 4–5 wk at 17°C. Ribbons of paired receptors are visible in a “defective” region along the length of the tube in *b* and in the small rounded end regions of the tubes in *c* and *d*. Note also the zones of densest staining on either side of the middle portions of the tubes (see Fig. 2). Bar, 0.1  $\mu\text{m}$ .  $\times 123,000$ .

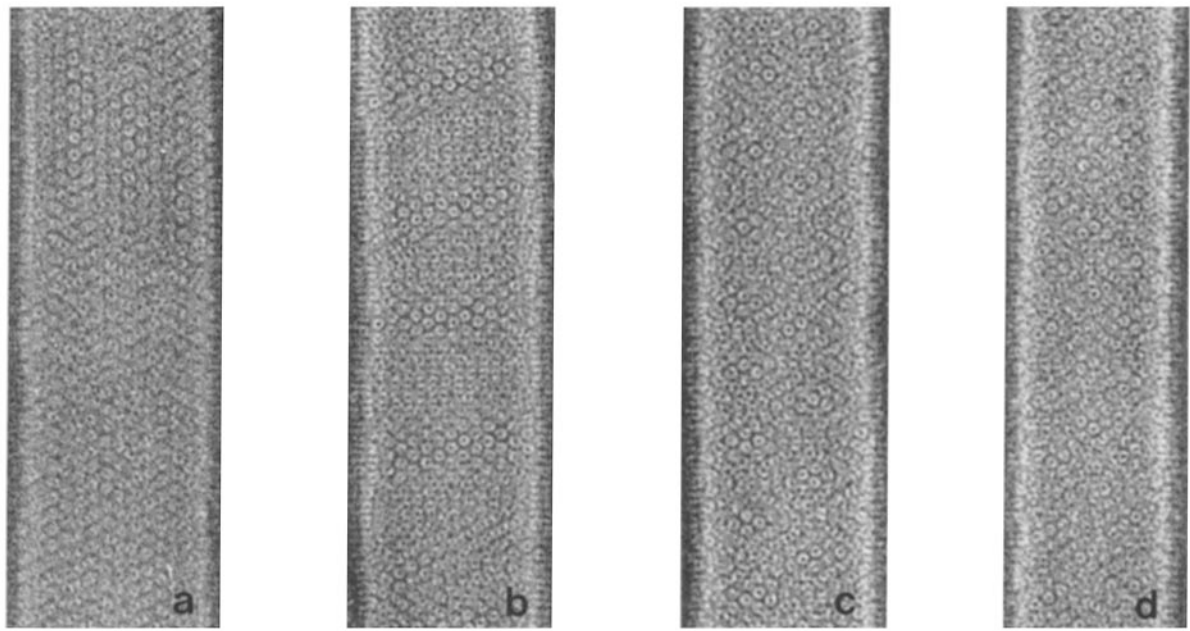


FIGURE 6 Detail from flattened tubes showing different superposition patterns formed by the two sides. (a) The surface lattice is oriented so that the (2,-4) line (Fig. 8) is approximately parallel to the tube axis; in *d* it is oriented so that the (2,-3) line is approximately parallel to the tube axis. *b* and *c* are intermediate orientations.  $\times 228,000$ .

conditions used for separating  $\delta$ - $\delta$  subunit-linked dimers from *Torpedo* in other studies (5). On the other hand, their organization and morphology were insensitive to prolonged exposure (10 min) of agonist ( $10^{-4}$  M carbamylcholine), as also found for the paired groupings of receptors on quick-frozen postsynaptic membranes of *Torpedo* (15).

Several structural observations suggest that tubes and ribbons may be related polymorphic forms. First, the initial occurrence of ribbons in a suspension was concurrent with the appearance of tubes; no suspension showed only one of these structures. Second, ribbons occasionally aligned obliquely over the vesicle surface, forming a loosely packed helical structure (Fig. 4*a*) which seems likely to be variant or precursor of the normal, compacted tube. Third, ribbons were often present on a tube-forming vesicle either in the rounded end region or in "defective regions" along the length of a tube (Figs. 4*b* and 5). Fourth, rows of receptors within the tubes were sometimes seen to be continuous with rows of receptors within the ribbons (Fig. 4*b*). Taken together, the observations could be seen as indicating that the tube is simply a cylinder made of laterally aggregated ribbons which are aligned obliquely to its axis. This conclusion is substantiated by the analysis below.

### The Surface Lattice

Images of the tubes present a wide range of patterns (Fig. 6) which result from superposition of details from the two sides. The reason for the complexity is apparent from their optical transforms (Fig. 7) which show only one kind of single-side reciprocal lattice but a range ( $\sim \pm 7^\circ$ ) in the orientation of this lattice relative to the axis of the tube. Thus there is only one basic surface lattice, but different superposition patterns arise because of the different orientations.

The surface lattice, defined by the geometry of the reciprocal lattice, is illustrated in Fig. 8*B*. There is a significant variation in the measured unit cell dimensions, the largest dimensions being associated with tubes of the type in Fig. 6*a*

and the smallest with those of the type in Fig. 6*d*. Average values based on eight independent measurements from Fig. 7 are:  $a = 89.7 \text{ \AA} (\pm 4.4 \text{ SD})$ ,  $b = 162.4 \text{ \AA} (\pm 6.0 \text{ SD})$ ,  $\gamma = 117.1^\circ (\pm 1.5 \text{ SD})$ . We note that the  $a$  and  $b$  dimensions would be nearly equivalent and the lattice would be approximately hexagonal if it were not for the fact that there is a doubling of the  $b$  dimension, indicated by the presence of weak "superlattice" peaks (see Materials and Methods) at positions midway between the major transform peaks (Figs. 7 and 8*A*).

### Projected Structure

Projection maps synthesized from uniformly flattened and well-preserved tubes (see Materials and Methods) all showed the same basic features (Fig. 9). We found that the receptors were grouped in pairs, their orientations within each pair being related by apparent dyad axes perpendicular to the plane of the membrane. This relationship was indicated by the matching asymmetric distributions of mass around the perimeters of the differently oriented receptors and by their matching pentagonal shapes. It was also manifest in the close to centrosymmetric phases of the transform peaks (Table I). The packing in the lattice must therefore have the symmetry of the plane group  $p2$  (as indicated in Fig. 9), rather than the lower asymmetry ( $p1$ ) assumed in the calculations.

An obvious deduction to be made from these maps is that the doubling of the  $b$  cell dimension (Fig. 8) is due simply to the dyad pairing of receptors along the (0,1) lines of the surface lattice. In addition, the appearance of rows of paired receptors within the tubes provides more direct evidence that tubes and ribbons (Fig. 4) are closely related polymorphic forms. Comparison of the rows of paired receptors in Fig. 9 with computer-filtered images of the ribbons (results not shown) suggests that the row indicated in Fig. 9, top, has the packing that is common to both structures. This row is least affected in terms of "bonding" geometry by small variations in lattice dimensions and also appears to contain the basic

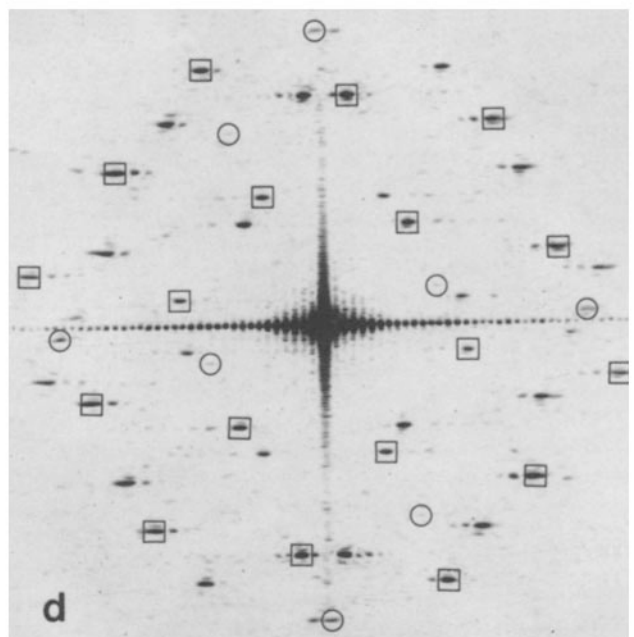
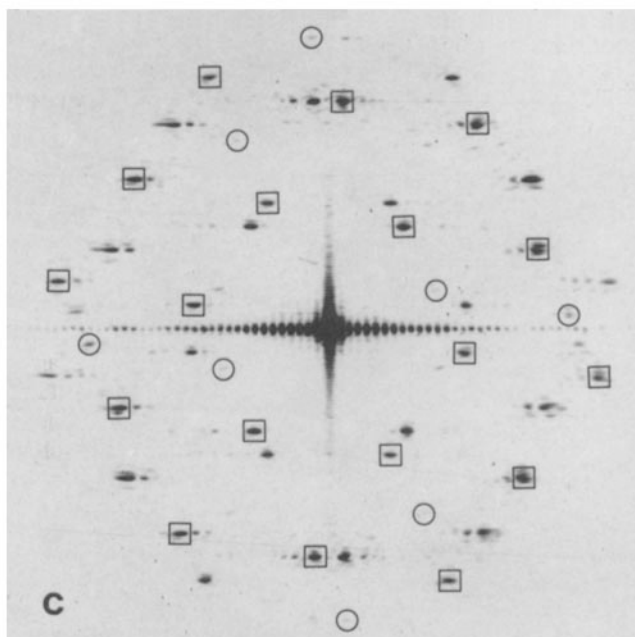
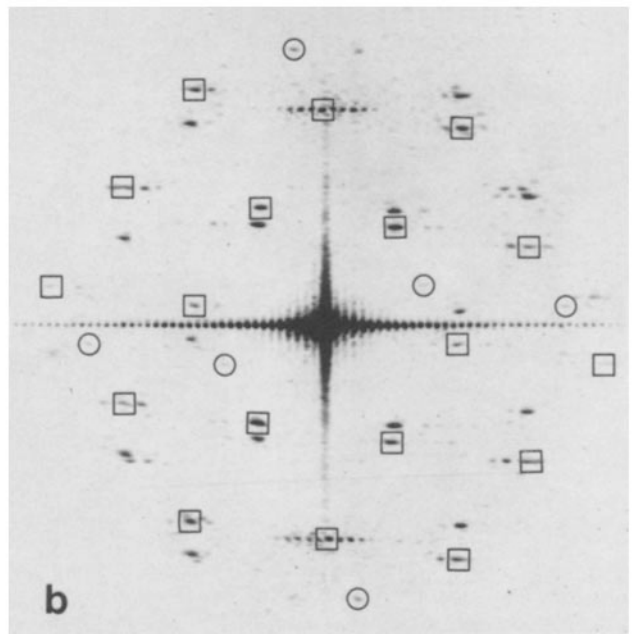
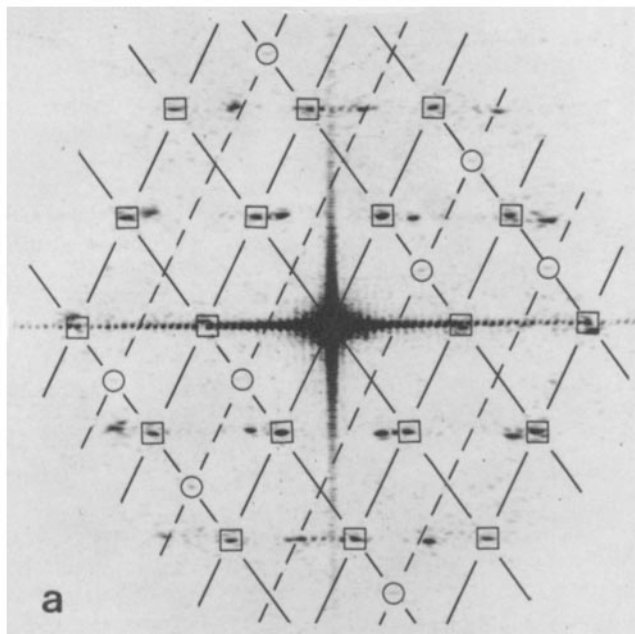


FIGURE 7 Optical transforms from tubes in Fig. 6, a–d, respectively. Peaks arising from one side of a tube lie on a lattice related to that of the other side by approximate mirror symmetry about a vertical line (direction of tube axis). In each example the peaks from just one side have been outlined; they are rotated differently relative to the tube axis in the different cases, reflecting variations in the orientation of the surface lattice. The strong peaks (squares) lie on a near-to-hexagonal net (full lines in a). There are also weak “superlattice” peaks (circles), lying in positions midway between the net points (along the broken lines in a), which are associated with a doubling of the  $b$  dimension of the unit cell (Fig. 9). Scale:  $1 \text{ cm} = 0.0076 \text{ \AA}^{-1}$ .

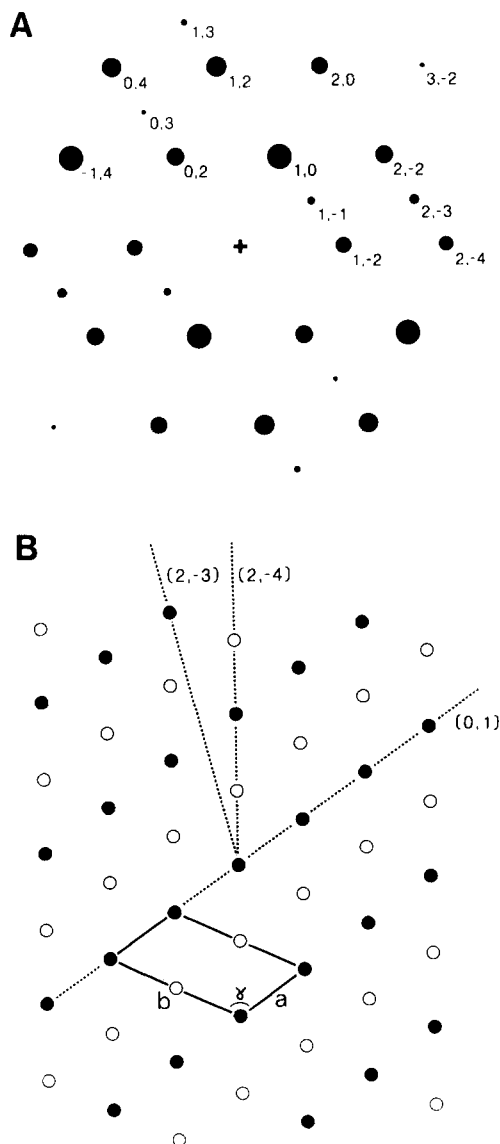


FIGURE 8 Diagrams of the Fourier transform (A) and surface lattice (B) of one side of a tube, viewed from the outside (with the hand determined as in Materials and Methods). Transforms computed from typical well-ordered tubes contain 14 independent  $h,k$  peaks, the amplitudes of which are proportional to the diameters in A (see also Table I). Certain other peaks, such as the 2,-1, are sometimes also apparent. Some lines of the surface lattice and the choice of unit cell used are indicated in B. The axes of most tubes lie within the directions defined by the (2,-3) and (2,-4) lines. Peaks for which  $k$  is odd ("superlattice" peaks) are associated with a doubling of the  $b$  dimension of the surface lattice (indicated by alternate rows of closed and open circles along the (0,1) lines).

structural dimer ( $AB$  in Fig. 9), based on receptor-receptor connectivity.

## DISCUSSION

Results showed that tubes are composed of oppositely oriented pairs of receptor molecules arranged on a crystalline surface lattice with the plane group symmetry  $p2$ . The pairs of receptors align in rows along the (0,1) line of the surface lattice (Fig. 8), a direction which makes an oblique angle to the axis of the tube. This angle was found to be somewhat

variable, giving rise to a wide range of superposition patterns from the two sides. The unit cell parameters also varied slightly, but the basic geometry of the packing did not change, indicating that all tubes are of one class. The appearance of ribbons composed of paired receptors on the surfaces of tube-forming vesicles, together with the equivalent configurations seen in projection maps, led us to conclude that the tubes grow by lateral aggregation of the ribbons.

It was not proven that the pairing in the tubes and ribbons involves interaction between the  $\delta$ -subunits through disulfide links, but this seems very likely for several reasons. First, ribbons and tubes were observed to be rapidly dispersed upon addition of small amounts of dithiothreitol. Second, the most likely candidates for the pairing (the receptors  $AB$  in Fig. 9) involve close apposition of the highest contour levels, as would be expected with the  $\delta$ -subunit being the largest of the five subunits. Third, the grouping of receptors in the ribbons and tubes bears a close resemblance to that seen in photographs of quick-frozen, deep-etched *Torpedo* postsynaptic membranes (15), where the receptors are presumably paired by the  $\delta$ - $\delta$  interactions.

In an earlier study of tubular crystals (17), prepared from the electric organ of *Torpedo californica*, it was proposed that the receptors arrange on a  $p1$  surface lattice (i.e., with all molecules pointing in the same direction), in contrast to what we have found. However, the receptors composing the tubes described earlier formed a less ordered, more loosely packed lattice, which did not permit as accurate an account to be given of their structure. We show here that there is actually a doubling of the  $b$  cell dimension, reflected in the appearance of weak "superlattice" peaks in optical transforms of the images. Analogous results were also obtained in a recent investigation of crystalline tubes of pentagonal capsomeres from polyoma virus, where the symmetry of the surface lattice is also of the plane group  $p2$  (2).

The twofold relation we observe can be used to give a measure of the accuracy of the projections in Fig. 9. In either example, the crystallographically related receptors differ from each other by less than the interval between contours, which implies that the maps do give a reliable representation of their stained structure. Thus the shown asymmetric distribution of mass and regular pentagonal shape are realistic features at the attained (30 Å) level of resolution. The results do not agree with other determinations (e.g., references 17, 24, 27, and 28), which suggest that the receptor has strongly fluctuating densities around its perimeter and/or looks like a horseshoe. However, in our initial selection of images (see Materials and Methods) we found that the receptor is very easily distorted by preparative procedures and by electron damage, factors that previously were not quantitatively evaluated.

It is interesting to find that the receptor has a characteristic, asymmetric distribution of mass around its perimeter, yet a strikingly regular pentagonal shape. This combination of features suggests that the five subunits may have slightly different lengths, but approximately equal cross sections. An equivalence of cross sections extending into the lipid bilayer would be consistent with the observed amino acid homology between the four polypeptides and would support the notion (12, 13, 21), that the transmembrane portions of the subunits share a common motif of secondary structure.

We thank Peter Ennis for his help and advice.

The research was supported by the European Molecular Biology

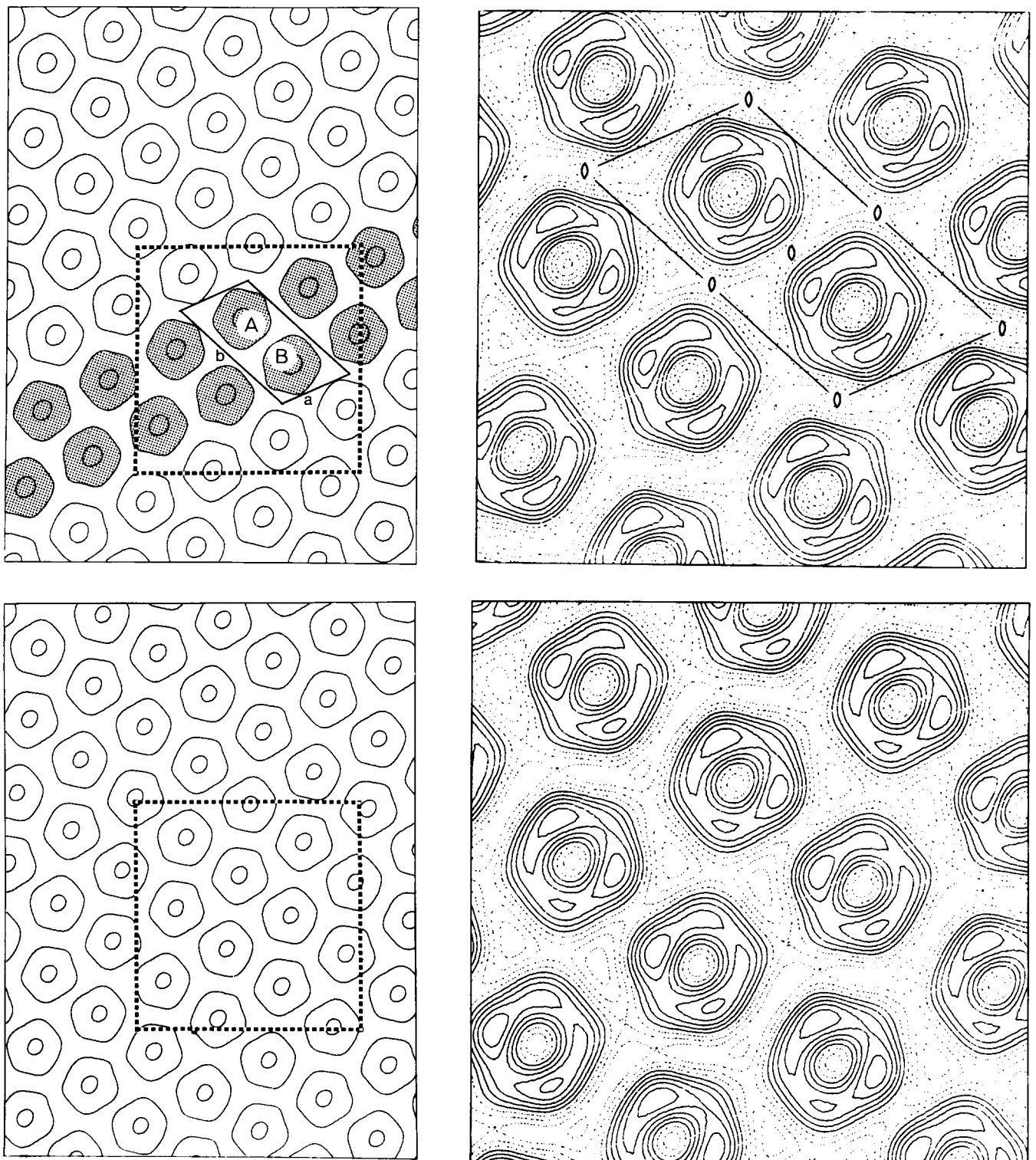


FIGURE 9 Maps showing the packing (left) and projected structures at 30 Å resolution (right) of receptors on the tube surface, determined from the structure factors listed in Table I. The view is from the outside of the tube (i.e., synaptic face uppermost) and all maps are oriented such that the tube axis is vertical. Continuous lines represent negative and zero contour levels (corresponding to stain-excluding regions); broken lines represent positive contour levels. The left-hand maps show zero contour levels only; packing in the region shaded may correspond to that in ribbons (Fig. 3), with the pair of receptors, AB, making the most significant contacts. The right-hand maps are of the areas outlined; the putative p2 plane group symmetry is indicated in the top right panel. The lattice dimensions in the top panels are  $a = 81.3 \text{ Å}$ ,  $b = 153.5 \text{ Å}$ , and  $\gamma = 114.4^\circ$ , and in the bottom  $a = 86.3 \text{ Å}$ ,  $b = 157.5 \text{ Å}$ , and  $\gamma = 116.4^\circ$ . These differences seem to reflect small differences between top and bottom maps in the packing of adjacent "ribbons."

Organization EMBO and Phillippe Foundation Fellowships to A. Brisson and a grant (GM27764) from the National Institutes of Health.

Received for publication 17 April 1984, and in revised form 4 June 1984.

## REFERENCES

1. Amos, L. A., R. Henderson, and P. N. T. Unwin. 1982. Three-dimensional structure determination by electron microscopy of two-dimensional crystals. *Prog. Biophys. Mol. Biol.* 39:183-231.
2. Baker, T. S., D. L. D. Caspar, and W. T. Murakami. 1983. Polyoma virus "hexamer" tubes consist of paired pentamers. *Nature (Lond.)* 303:446-448.
3. Brisson, A. 1980. Etude structurale de proteines membranaires au moyen des methodes optiques et numeriques d'analyse d'images de microscopie electronique. Ph.D. Thesis. University of Grenoble. 1-77.
4. Cartaud, J., E. L. Benedetti, A. Sobel, and J.-P. Changeux. 1978. A morphological study of the cholinergic receptor protein from *Torpedo marmorata* in its membrane environment and in its detergent-extracted purified form. *J. Cell Sci.* 29:313-337.
5. Chang, H. W., and E. Bock. 1977. Molecular forms of acetylcholine receptor. Effects of calcium ions and a sulfhydryl reagent on the occurrence of oligomers. *Biochemistry* 16:4513-4520.
6. Changeux, J.-P. 1980. The acetylcholine receptor: an "allosteric" membrane protein. *Harvey Lect.* 75:85-254.
7. Claudio, T., M. Ballivet, J. Patrick, and S. Heinemann. 1983. Nucleotide and deduced amino acid sequences of *Torpedo californica* acetylcholine receptor  $\gamma$  subunit. *Proc. Natl. Acad. Sci. USA* 80:1111-1115.
8. Conti-Tronconi, B. M., and M. A. Raftery. 1982. The nicotinic cholinergic receptor: correlation of molecular structure with functional properties. *Annu. Rev. Biochem.* 51:491-530.
9. DeRosier, D. J., and P. B. Moore. 1970. Reconstruction of three-dimensional images from electron micrographs of structures with helical symmetry. *J. Mol. Biol.* 52:355-369.
10. Devillers-Thiery, A., J. Giraudat, M. Bentaboulet, J.-P. Changeux. 1983. Complete mRNA coding sequence of the acetylcholine binding  $\alpha$ -subunit of *Torpedo marmorata* acetylcholine receptor: a model for the transmembrane organization of the polypeptide chain. *Proc. Natl. Acad. Sci. USA* 80:2067-2071.
11. Finch, J. T., and A. Klug. 1965. The structure of viruses of the Papilloma-Polyoma type. III. Structure of rabbit Papilloma virus. *J. Mol. Biol.* 13:1-12.
12. Finer-Moore, J., and R. M. Stroud. 1984. Amphipathic analysis and possible formation of the ion channel in an acetylcholine receptor. *Proc. Natl. Acad. Sci. USA* 81:155-159.
13. Guy, H. R. 1984. A structural model of the acetylcholine receptor channel based on partition energy and helix packing calculations. *Biophys. J.* 45:249-261.
14. Hamilton, S. L., M. McLaughlin, and A. Karlin. 1977. Disulfide bond cross-linked dimer in acetylcholine receptor from *Torpedo californica*. *Biochem. Biophys. Res. Commun.* 79:692-699.
15. Heuser, J. E., and S. R. Salpeter. 1979. Organization of acetylcholine receptors in quick-frozen, deep-etched, and rotary-replicated *Torpedo* postsynaptic membrane. *J. Cell Biol.* 82:150-173.
16. Karlin, A. 1980. Molecular properties of nicotinic acetylcholine receptors. In *The Cell Surface and Neuronal Function*. C. W. Cotman, G. Poste, and G. L. Nicolson, editors. Elsevier/North Holland Biomedical Press, Amsterdam. 191-260.
17. Kistler, J., and R. M. Stroud. 1981. Crystalline arrays of membrane-bound acetylcholine receptor. *Proc. Natl. Acad. Sci. USA* 78:3678-3682.
18. Klymkowsky, M. W., and R. M. Stroud. 1979. Immunosppecific identification and three-dimensional structure of a membrane-bound receptor from *Torpedo californica*. *J. Mol. Biol.* 128:319-334.
19. Noda, M., H. Takahashi, T. Tanabe, M. Toyosato, Y. Furutani, T. Hirose, M. Asai, S. Inayama, T. Miyata, and S. Numa. 1982. Primary structure of  $\alpha$ -subunit precursors of *Torpedo californica* acetylcholine receptor deduced from cDNA sequences. *Nature (Lond.)* 299:793-797.
20. Noda, M., H. Takahashi, T. Tanabe, M. Toyosato, S. Kikuyotani, T. Hirose, M. Asai, H. Takashima, S. Inayama, T. Miyata, and S. Numa. 1983. Primary structure of the  $\beta$ - and  $\delta$ -subunit precursors of *Torpedo californica* acetylcholine receptor deduced from cDNA sequences. *Nature (Lond.)* 301:251-255.
21. Noda, M., H. Takahashi, T. Tanabe, M. Toyosato, S. Kikuyotani, Y. Furutani, T. Hirose, H. Takashima, S. Inayama, T. Miyata, S. Numa. 1983. Structural homology of *Torpedo californica* acetylcholine receptor subunits. *Nature (Lond.)* 302:528-532.
22. Popot, J.-L., and J.-P. Changeux. 1984. The nicotinic receptor of acetylcholine: structure of an oligomeric integral membrane protein. *Physiol. Rev.* In press.
23. Raftery, M. A., M. W. Hunkapiller, C. D. Strader, and L. E. Hood. 1980. Acetylcholine receptor: complex of homologous subunits. *Science (Wash. DC)* 208:1454-1457.
24. Ross, M. J., M. W. Klymkowsky, D. A. Agard, and R. M. Stroud. 1977. Structural studies of a membrane-bound acetylcholine receptor from *Torpedo californica*. *J. Mol. Biol.* 116:635-659.
25. Unwin, P. N. T., and R. Henderson. 1975. Molecular structure determination by electron microscopy of unstained crystalline specimens. *J. Mol. Biol.* 94:425-440.
26. Wrigley, N. G. 1968. The lattice spacing of crystalline catalase as an internal standard of length in electron microscopy. *J. Ultrastruct. Res.* 24:454-464.
27. Zingsheim, H.-P., D.-C. Neugebauer, F. J. Barrantes, and J. Frank. 1980. Structural details of membrane-bound acetylcholine receptor from *Torpedo marmorata*. *Proc. Natl. Acad. Sci. USA* 77:952-956.
28. Zingsheim, H.-P., D.-C. Neugebauer, J. Frank, W. Hänicke, and F. J. Barrantes. 1982. Dimeric arrangement and structure of the membrane-bound acetylcholine receptor studied by electron microscopy. *EMBO (Eur. Mol. Biol. Organ.) J.* 1:541-547.